Journal of Modern Optics
Vol. 00, No. 00, 10 January 2008, 1–20

RESEARCH ARTICLE

A Mixed Hybrid Finite Element Method for the Helmholtz Equation

A. Hannukainen, M. Huber and J. Schöberl
(*Received 00 Month 200x; final version received 00 Month 200x*)

In this paper, a high order hybrid mixed finite element method for solving the two dimensional Helmholtz equation with high wave numbers is presented. The novelty of this method is in using a discrete eigenfunction basis for solving the hybrid problem. Such basis allows inexpensive elimination of the inner degrees of freedom, which considerably reduces the size of the resulting linear system. On a rectangular grid with hanging nodes, the eigenfunction basis is constructed by solving a one dimensional eigenvalue problem for each pair of edge length and polynomial order in the mesh. The eigenvalue problem can be solved efficiently for polynomial orders up to thousand. Together with the reduced size of the linear system, this makes it possible to work with very high order basisfunctions, and consequently high frequency waves can be resolved on a coarse mesh. The *hp*−refinement is used to obtain accurate solutions for minimal number of degrees of freedom. The effectiveness of our approach is demonstrated with numerical examples using polynomials of the degree up to thousand.

1. Introduction

The solution of the Helmholtz equation is of high interest for time harmonic wave propagation problems in electrodynamics, especially in optics and in acoustics, hence a large variety of different solution methods has been developed for it. For problems posed in homogenus media, e.g. scattering problems, integral equation methods are widely used. However, these methods are not well suited for problems in non-homogenous media. For such problems, finite differences (*17*), finite volumes (*20*), the Trefftz method (*21*), and finite element methods (FEM) are more efficient.

When applied to wave-type problems, such as the Helmholtz equation, the standard finite element method suffers form two major difficulties. The first difficulty is the rapid growth in the number of degrees of freedom required to accurately solve wave-problems with high wavenumbers and frequencies ω. For example, for two dimensional Helmholtz equation, the number of unknowns grows due to the pollution error (*18, 19*) faster than $\mathcal{O}\left(\omega^2\right)$. The most efficient approach to control this growth is the *hp* refinement (*2, 14, 24*). The second difficulty standard FEM faces, is the lack of good preconditioned iterative schemes for solving the resulting linear system. Some advances in preconditioners have been made (*15*), but efficient precondioners for wave-type problems do not exist at the moment.

Due to the difficulties faced by standard finite elements, a large variety of different approaches for solving the time-harmonic wave propagation problems within the FEM framework have been developed. The most popular ones are *hp* FEM (*18*), the least squares methods (*23*), the partition of unity method (*4*), the discontinuous Galerkin method (*3, 16*), and the ultra weak variational formulation (*7, 8*). Our work is based on a hybrid mixed finite element method from (*22*) and it is motivated by hybrid finite element methods for the Laplace equation (*6, 11, 12*).

In hybrid mixed finite element methods, the normal continuity of the flux is broken across the element interfaces and enforced again by introducing Lagrangian multipliers, supported on

*Institute of Mathematics, Helsinki University of Technology, P.O.Box 1100, FI-02015 TKK, Finland (ahannuka@cc.hut.fi)
†Center for Computational Engineering Science, RWTH Aachen, Pauwelsstraße 19, 52074 Aachen, Germany, (huber@mathcces.rwth-aachen.de, joachim.schoeberl@rwth-aachen.de)

ISSN: 0950-0340 print/ISSN 1362-3044 online

DOI: 10.1080/0950034YYxxxxxxxx
http://www.informaworld.com

the facets. The hybridization of the mixed Helmholtz equation is more involved. In addition to breaking the continuity of the flux, a second Lagrange multiplier has to be introduced. Without this Lagrange multiplier, the interior degrees of freedom cannot be eliminated (see (*22*)). For Helmholtz equation, the Lagrange multipliers represent the scalar field E and the normal flux $\mathbf{H}\cdot\mathbf{n_F}$ on the facets. In the following, unknowns related to the E and $\mathbf{H}$ fields are called interior degrees of freedom and unknowns related to Lagrange multipliers we call facet degrees of freedom.

After hybridization, each interior basis function is supported only on a single element. Thus, there is no coupling between interior degrees of freedom of different elements, and these degrees of freedom can be eliminated element by element. Such elimination reduces the original linear system to a considerably smaller Schur complement problem for the facet unknowns.

The novelty of our method is in using a discrete eigenfunction basis, which makes both the assembly of the system matrix and the elimination of the interior degrees of freedom, i.e. reduction to Schur complement problem, computationally inexpensive. On rectangular meshes with hanging nodes, such a basis is constructed by solving a one dimensional eigenvalue problem for each pair of edge lengths and polynomial orders in the mesh. The eigenvalue problem can be solved for polynomial orders up to thousands, which together with the cheap assembly and the reduction in problem size make it possible to use very high order basisfunctions. To obtain exponential convergence rates, we will use this approach together with *hp* refinement.

The paper is organized as follows: In section 2 the mixed hybrid formulation is derived and discussed. Section 3 states the one dimensional eigenvalue problem, which leads to the basisfunctions for the interior degrees of freedom. The section concludes with a detailed discussion of the properties of the resulting system of linear equations. The solution strategy for the linear system of equations obtained after elimination of the inner degrees of freedom is treated in section 4. Section 5 is devoted to hanging nodes. We discuss the consequences of hanging nodes onto the assembly procedure and the preconditioner. The paper concludes with numerical examples in section 6.

2. The mixed hybrid formulation

In this section, we present the mixed hybrid formulation of the Helmholtz equation. The hybrid formulation is derived from the mixed problem:
Find a scalar field $E(x,y)$ and a vector valued field $\mathbf{H}(x,y)$ such that

$$\begin{aligned} \operatorname{grad} E &= i\omega\,\mu\,\mathbf{H} \\ \operatorname{div}\mathbf{H} &= i\omega\,\epsilon\,E \end{aligned} \qquad \text{in } \Omega \tag{1}$$

with Dirichlet, Neumann, or absorbing boundary conditions

$$E = E_d, \quad \mathbf{H}\cdot\mathbf{n_\Omega} = H_n, \quad \mathbf{H}\cdot\mathbf{n_\Omega} = \sqrt{\frac{\epsilon}{\mu}}\,(E - 2\,E_{in}) \tag{2}$$

prescibed on Γ_d, Γ_n and Γ_a, respectively.

Here Ω is a bounded domain in $\mathbb{R}^2$ with sufficiently regular boundary $\partial\Omega = \Gamma_a \cup \Gamma_n \cup \Gamma_d$. The outer normal of Ω is denoted by $\mathbf{n_\Omega}$. The functions H_n, E_{in}, and E_d are from the spaces $L^2(\Gamma_n)$, $L^2(\Gamma_a)$, and $L^2(\Gamma_d)$. The parameter ϵ is a piecewise constant function, and $\omega, \mu \in \mathbb{R}^+$. For applications in electromagnetics, E and $\mathbf{H}$ are equivalent to the electric and magnetic fields for transverse electric modes, ω is the angular frequency, μ the magnetic permeability, and ϵ the electric permittivity.

Before stating the hybrid formulation, we need some additional definitions. The domain Ω is

approximated by a triangulation $\mathcal{R}$. The set of interior and boundary edges of $\mathcal{R}$ are called its facets and denoted by $\mathcal{F}$. The parameter ϵ is assumed to be constant on each element $R \in \mathcal{R}$. The required function spaces are denoted as

$$\begin{aligned} U = L^2(\mathcal{R}) &:= L^2(\Omega) \\ V = H(\mathrm{div}, \mathcal{R}) &:= \left\{ \mathbf{v} \in \left(L^2(\mathcal{R})\right)^2 \,:\, \mathrm{div}\, \mathbf{v}|_R \in L^2(R) \qquad \forall R \in \mathcal{R} \right\}, \\ U_F = L^2(\mathcal{F}) &:= \left\{ u \,:\, u|_F \in L^2(F) \qquad \forall F \in \mathcal{F} \right\} \end{aligned}$$

and

$$W = U \times V \times U_F \times U_F.$$

We will use the notation

$$\int_R u(\mathbf{x})\, v(\mathbf{x})\, d\mathbf{x} = \big(u, v\big)_R \qquad \text{and} \qquad \int_{\partial R} u(\mathbf{x})\, v(\mathbf{x})\, ds = \big\langle u, v \big\rangle_{\partial R}.$$

for element and edge integrals. The outer normal of the element $R \in \mathcal{R}$ is denoted by $\mathbf{n_R}$ and normal to the facet $F \in \mathcal{F}$ by $\mathbf{n_F}$. For inner facets $\mathbf{n_F}$ is equal to one of the outer normal vectors $\mathbf{n_R}$ of the two neighboring elements and on boundary facets $\mathbf{n_F} = \mathbf{n_R} = \mathbf{n_\Omega}$.

Using the above definitions, the weak form of the hybrid mixed problem is

Problem 2.1 Find $u = (E, \mathbf{H}, E_F, H_F) \in W$ such that

$$\tilde{a}(u, v) = \tilde{f}(v) \qquad \forall v = (e, \mathbf{h}, e_F, h_F) \in W$$

with the bilinear form

$$\begin{aligned} \tilde{a}(u, v) = \sum_{R \in \mathcal{R}} \big[&-\big(E, \mathrm{div}\, \mathbf{h}\big)_R - i\omega\mu\big(\mathbf{H}, \mathbf{h}\big)_R - \big(\mathrm{div}\, \mathbf{H}, e\big)_R + i\omega\epsilon\big(E, e\big)_R \\ &+\big\langle E_F, \mathbf{h} \cdot \mathbf{n_R} \big\rangle_{\partial R} + \big\langle \mathbf{H} \cdot \mathbf{n_R}, e_F \big\rangle_{\partial R} + \beta \big\langle \mathbf{H} \cdot \mathbf{n_F} - H_F, \mathbf{h} \cdot \mathbf{n_F} - h_F \big\rangle_{\partial R} \big] \\ &-\big\langle \sqrt{\epsilon/\mu}\, E_F, e_F \big\rangle_{\Gamma_a} - \big\langle H_F, e_F \big\rangle_{\Gamma_d} - \big\langle E_F, h_F \big\rangle_{\Gamma_d} \end{aligned} \tag{3}$$

and linear functional

$$\tilde{f}(v) = -2\big\langle \sqrt{\epsilon/\mu}\, E_{in}, e_F \big\rangle_{\Gamma_a} + \big\langle H_n, e_F \big\rangle_{\Gamma_n} - \big\langle E_d, h_F \big\rangle_{\Gamma_d}. \tag{4}$$

Here, the parameter $\beta \in \mathbb{C}$ is an arbitrary stabilization parameter. The solution of this problem is equivalent to the solution of the mixed problem (see (*22*)).

Lemma 2.2: *Let $(E_e, \mathbf{H}_e)$ be the exact solution of (1) with appropriate boundary conditions, and let $E_F^e = E^e$ as well as $H_F^e = \mathbf{H}^e \cdot \mathbf{n_F}$ on the facets. Then $u_e = (E^e, \mathbf{H}^e, E_F^e, H_F^e)$ solves problem 2.1.*

Proof: Inserting u_e to problem 2.1 and using the definition of boundary conditions (2), we obtain

$$\sum_{R\in\mathcal{R}} \big[-\big(E^e, \operatorname{div}\mathbf{h}\big)_R - i\omega\mu\big(\mathbf{H}^e, \mathbf{h}\big)_R - \big(\operatorname{div}\mathbf{H}^e, e\big)_R + i\omega\epsilon\big(E^e, e\big)_R + \big\langle E_F^e, \mathbf{h}\cdot\mathbf{n_R}\big\rangle_{\partial R} + \big\langle \mathbf{H}^e\cdot\mathbf{n_R}, e_F\big\rangle_{\partial R}\big] - \big\langle \mathbf{H}^e\cdot\mathbf{n_\Omega}, e_F\big\rangle_{\partial\Omega} = 0.$$

Due to the continuity of the normal component of $\mathbf{H}^e$, the integrals $\big\langle \mathbf{H}^e\cdot\mathbf{n_R}, e_F\big\rangle_{\partial R}$ cancel on all inner edges. On boundary edges this term cancels with the boundary integrals. Exchanging E_F^e by E^e yields

$$\sum_{R\in\mathcal{R}} \big[-\big(E^e, \operatorname{div}\mathbf{h}\big)_R + \big\langle E^e, \mathbf{h}\cdot\mathbf{n_R}\big\rangle_{\partial R} - i\omega\mu\big(\mathbf{H}^e, \mathbf{h}\big)_R - \big(\operatorname{div}\mathbf{H}^e, e\big)_R + i\omega\epsilon\big(E^e, e\big)_R\big] = 0.$$

Integration by parts gives

$$\sum_{R\in\mathcal{R}} \big[\big(\operatorname{grad}E^e - i\omega\mu\mathbf{H}^e, \mathbf{h}\big)_R - \big(\operatorname{div}\mathbf{H}^e - i\omega\epsilon E^e, e\big)_R\big] = 0,$$

which completes the proof. □

In (*22*) problem 2.1 is discretized by using a broken Raviart Thomas space. We will follow the same approach, but instead of E_F, H_F we introduce "incoming" and "outgoing" wave contributions of E, called G_I and G_O, which are defined as

$$H_F = (\mathbf{n_R}\cdot\mathbf{n_F})\sqrt{\frac{\tilde{\epsilon}}{\mu}}\,(G_O - G_I) \quad \text{and} \quad E_F = (G_O + G_I)\,.$$

The parameter $\tilde{\epsilon}$ is the mean of ϵ on the two neighboring elements. If there is a jump in the coefficient ϵ across element edges, the physical incoming and outgoing waves are not equal with G_O and G_I. Note that the wave outgoing form element R , G_O, is equal to the wave incoming to the neighboring element, G_I, and vice versa. Consequently H_F has the same sign on every element in spite of the sign change of $\mathbf{n_R}\cdot\mathbf{n_F}$. On the boundary $\mathbf{n_R}\cdot\mathbf{n_F}$ equals one, and G_I and G_O are the waves incoming and outgoing from the whole domain. Inserting these new unknowns to problem 2.1 results in the following problem formulation:

Problem 2.3 Find $(E, \mathbf{H}, G_I, G_O) =: u \in W$ such that

$$a_I(u,v) + a_{IF}(u,v) + a_{IF}(v,u) + a_F(u,v) = f(v) \qquad \forall v = (e, \mathbf{h}, g_I, g_O) \in W$$

with the bilinear form for the inner degrees of freedom

$$a_I(u,v) := \sum_{R\in\mathcal{R}} \big[i\omega\epsilon\big(E, e\big)_R - \big(\operatorname{div}\mathbf{H}, e\big)_R - \big(E, \operatorname{div}\mathbf{h}\big)_R - i\omega\mu\big(\mathbf{H}, \mathbf{h}\big)_R + \beta\big\langle \mathbf{H}\cdot\mathbf{n_R}, \mathbf{h}\cdot\mathbf{n_R}\big\rangle_{\partial R}\big]\,, \tag{5}$$

the bilinear form for the facet degrees of freedom

$$a_F(u,v) := \sum_{R\in\mathcal{R}} \beta\langle\tilde{\epsilon}/\mu\,(G_O - G_I),(g_O - g_I)\rangle_{\partial R} \tag{6}$$
$$- \langle\sqrt{\tilde{\epsilon}/\mu}\,(G_O + G_I),(g_O + g_I)\rangle_{\Gamma_a} - \langle 2\sqrt{\tilde{\epsilon}/\mu}\,G_O, g_O\rangle_{\Gamma_d} + \langle 2\sqrt{\tilde{\epsilon}/\mu}\,G_I, g_I\rangle_{\Gamma_d},$$

the bilinear form coupling inner and facet variables

$$a_{IF}(u,v) := \sum_{R\in\mathcal{R}} \left[\langle\left(1-\beta\sqrt{\tilde{\epsilon}/\mu}\right)G_O, \mathbf{h}\cdot\mathbf{n_R}\rangle_{\partial R} + \langle\left(1+\beta\sqrt{\tilde{\epsilon}/\mu}\right)G_I, \mathbf{h}\cdot\mathbf{n_R}\rangle_{\partial R}\right] \tag{7}$$

and the linear functional

$$f(v) := -2\langle\sqrt{\tilde{\epsilon}/\mu}\,E_{in},(g_O+g_I)\rangle_{\Gamma_a} + \langle E_n,(g_O+g_I)\rangle_{\Gamma_n} - \langle\sqrt{\tilde{\epsilon}/\mu}\,E_d,(g_O-g_I)\rangle_{\Gamma_d}.$$

The above problem is complex symmetric. If there is no jump in ϵ across element interfaces, i.e. $\epsilon = \tilde{\epsilon}$, we can choose $\beta = \sqrt{\frac{\mu}{\epsilon}}$ so that there is no coupling between inner degrees of freedom and outgoing waves. The physical interpretation is, that if there is no jump in ϵ at the interface, no reflections are present, and the field in the interior of an element depends only on the incoming waves.

Until now, we have not made any assumptions on the mesh. As we will later see, on a structured rectangular mesh with hanging nodes, the interior unknowns can be easily eliminated. However, for simplicity, we will begin by consider a rectangular mesh $\mathcal{R}$, such that every $R \in \mathcal{R}$ can be written as

$$R = I_x^R \times I_y^R = [q_x^R, q_x^R + h_x^R] \times [q_y^R, q_y^R + h_y^R], \tag{8}$$

where h_x and h_y are the width and height of the rectangle, and $\left(q_x^R, q_y^R\right)$ is the lower left vertex of R. The mesh with hanging nodes will be considered later

On such a mesh, two dimensional polynomial basisfunctions can be represented as a product of one dimensional polynomials. Upon this we define the discrete functionspace U_{hp} corresponding to U

$$U_{hp} = \prod_{R\in\mathcal{R}} P^{p_x}(I_x^R) \otimes P^{p_y}(I_y^R).$$

Here $P^p(I)$ is the set of all polynomials of order less or equal to p on the interval I. We use polynomial order p_x for x direction and order p_y for y direction. For the broken Raviart Thomas space V_{hp} we get

$$V_{hp} = \prod_{R\in\mathcal{R}} \left(P^{p_x+1}(I_x^R) \otimes P^{p_y}(I_y^R)\right) \times \left(P^{p_x}(I_x^R) \otimes P^{p_y+1}(I_y^R)\right),$$

and for the discrete version of U_F

$$U_{F,hp} = \prod_{F\in\mathcal{F}} P^{p_F}(F),$$

where p_F equals p_x for horizontal facets (parallel to the x-axis) and $p_F = p_y$ for vertical facets (parallel to the y-axis). We will solve problem 2.3 on the finite element space $W_{hp} = U_{hp} \times V_{hp} \times U_{F,hp} \times U_{F,hp}$.

3. The eigenfunction basis

In this section we present a discrete eigenfunction basis for the spaces U_{hp}, V_{hp} and $U_{F,hp}$. Such a basis reduces the contribution of the interior bilinear form $a_I(u,v)$ in the system matrix to three by three block diagonal. Consequently, the interior degrees of freedom can be easily eliminated, which leads to a considerably smaller Schur complement problem for the facet degrees of freedom. In addition, all integrals can be evaluated a priori, and costly numerical integration for high-order polynomials is not needed.

On a uniform rectangular mesh, constructing the eigenfunction basis requires solving two one dimensional eigenvalue problems. The computational work required to solve these problems is $O(p^3)$, where $p = \max\{p_x, p_y\}$. A Similar construction is not possible on unstructured meshes. In fact, on such meshes the eigenbasis has to be constructed elementwise, and it has computational cost $O(p^6)$ for each element. Such a construction would be much more costly than solving the original problem.

The basisfunctions for interior and facet degrees of freedom are defined via the eigenfunctions of the one dimensional eigenvalue problem

Problem 3.1 Find the eigenfunctions $\Psi_j(s) \in P^{p+1}(I)$ and the corresponding eigenvalues $\lambda_j \in \mathbb{C}$ for $1 \le j \le (p+2)$ such that

$$\int_I \Psi_j' \psi' \, ds = \lambda_j \mathcal{B}_h\big(\Psi_j, \psi\big) \qquad \forall \psi \in P^{p+1}(I)$$

where

$$\mathcal{B}_h\big(\Psi_j, \psi\big) = \int_I i\omega\mu \Psi_j \psi \, ds - \beta\big(\Psi_j(q)\psi(q) + \Psi_j(q+h)\psi(q+h)\big).$$

The eigenfunctions are orthogonal and they are normalized such that $\mathcal{B}_h\big(\Psi_j, \Psi_k\big) = \delta_{jk}$. Note, that the eigenfunction corresponding to the zero eigenvalue will be constant. In the following, the constant eigenfunction is denoted by the index $j = p+2$.

Problem 3 is solved by expanding the eigenfunctions into an integrated Legendre polynomial basis $Q_I^i(s)$ transformed to the interval $I = [q, q+h]$, which is of order $i < (p+1)$. Like Legendre polynomials, the integrated Legendre polynomials can be generated by a three term recurrence and due to orthogonality properties, they lead to a sparse, well conditioned matrix system for the problem . This matrix system reads as

Problem 3.2 Find $\mathbf{\Psi_j} \in \mathbb{C}^{p+2}$ and $\lambda_j \in \mathbb{C}$ such that

$$D \, \mathbf{\Psi_j} \;=\; \lambda_j \, M \, \mathbf{\Psi_j}$$

and $\mathbf{\Psi_j}^T M \mathbf{\Psi_k} = \delta_{jk}$. The elements of the diagonal matrix $D \in \mathbb{C}^{(p+2)\times(p+2)}$ are

$$D_{jj} = \frac{4}{h(2j-3)}$$

and the non-zero entries of $M \in \mathbb{C}^{(p+2)\times(p+2)}$

$$M_{jj} = \begin{cases} \frac{i\omega\mu h}{(2j-3)^2(2j-1)} - 2\beta & j = 1,2 \\ \frac{2i\omega\mu h}{(2j-5)(2j-3)(2j-1)} & \text{else} \end{cases}$$

$$M_{j\,j+2} = M_{j+2\,j} = \frac{-i\omega\mu h}{(2j-3)(2j-1)(2j+1)} \qquad \text{for } 1 \le j \le p.$$

Due to the orthogonality properties for the Integrated Legendre polynomials, this eigenvalue problem decouples into an "odd" and an "even" problem. These eigenvalue problems are smaller and therefore faster to solve.

The eigenfunctions are

$$\begin{aligned} \Psi_j(s) &= \sum_{k=0}^{p+1} \left(\mathbf{\Psi_j}\right)_{k+1} Q_I^k(s) \\ \Psi_j'(s) &= \sum_{k=1}^{p+1} \left(\mathbf{\Psi_j}\right)_{k+1} Q_I^{k\,\prime}(s) = \frac{2}{h} \sum_{k=0}^{p} \left(\mathbf{\Psi_j}\right)_{k+2} L_I^k(s) \end{aligned} \tag{9}$$

where $L_I^k(s)$ is the Legendre polynomial of the order k on the inteval I. Using these eigenfunctions, we can define the basis functions for spaces U_{hp} and V_{hp} as follows

Definition 3.3: Let R be a rectangle in $\mathcal{R}$ according to (8), then for $1 \le j \le (p_x+2)$ and $1 \le k \le (p_y+2)$ the basis functions of U_{hp} are defined as

$$e_{jk}(x,y) = \begin{cases} \Theta_j'(x)\Phi_k'(y) & \text{for } (x,y) \in R \\ 0 & \text{else} \end{cases}$$

and the basis functions of V_{hp} as

$$\mathbf{h^x}_{jk}(x,y) = \begin{cases} \left(\Theta_j(x)\Phi_k'(y), 0\right)^T & \text{for } (x,y) \in R \\ \mathbf{0} & \text{else} \end{cases}$$

$$\mathbf{h^y}_{jk}(x,y) = \begin{cases} \left(0, \Theta_j'(x)\Phi_k(y)\right)^T & \text{for } (x,y) \in R \\ \mathbf{0} & \text{else} \end{cases}.$$

The functions Θ_j are the eigenfunctions of Problem 3 with the eigenvalue $\lambda_j^x,\ p = p_x,\ I = I_x^R$, and Φ_k is an eigenfunction of the same problem with $I = I_y^R, p = p_y$ and eigenvalue λ_k^y.

In the above definition, all basisfunctions corresponding to the derivative of the constant eigenfunction are zero. These basisfunctions are kept for notational convinience, and can be omitted in the actual implementation. The basis functions for the facets are defined similar to Definition 3.3.

Definition 3.4: Let $F \in \mathcal{F}$ be a facet with $F = I^F = [\tilde{q}, \tilde{q}+\tilde{h}]$ and polynomial order p^F. The basis functions for $U_{F,hp}$ on the facet are

$$g_{O\,j} = g_{I\,j} = \begin{cases} \Xi_j' & \text{on } F \\ 0 & \text{else} \end{cases}$$

for $1 \le j \le p^F + 1$. Here Ξ_j is the eigenfunction of Problem 3 corresponding to the non-zero eigenvalue $\tilde{\lambda}_j$ with $p = p^F$ and $I = I^F$.

Note that for the constant eigenfunction $\Xi'_{p^F+2} = 0$, hence it is not needed in the definition. On a rectangle R, the polynomial order p^F and the interval I_F are equal to p_x and I_x^R for horizontal edges, and to p_y and I_y^R for vertical edges.

3.1. *The bilinear form $a_I(u, v)$*

As each interior basisfunction is supported only on a single element, the bilinear form $a_I(u, v)$ can be studied element by element. On an element R the contribution of $a_I(u, v)$ to the system matrix is

$$A^R = \begin{pmatrix} A^R_{EE} & A^R_{EH_x} & A^R_{EH_y} \\ A^R_{H_xE} & A^R_{H_xH_x} & A^R_{H_xH_y} \\ A^R_{H_yE} & A^R_{H_yH_x} & A^R_{H_yH_y} \end{pmatrix}, \tag{10}$$

where A^R_{EE} collects the coupling elements of the basis functions e_{jk} with themselves, $A^R_{EH_x}$ collects the coupling of the functions e_{jk} with $\mathbf{h^x_{mn}}$, and so on. All of the blocks have the dimension $(p_x+2)(p_y+2)\times(p_x+2)(p_y+2)$. We will use the notation $\big(A^R_{EE}\big)_{jk,mn}$ for the matrix element $\big(A^R_{EE}\big)_{(j(p_y+2)+k,m(p_y+2)+n)}$. This notation is used for all the blocks.

Lemma 3.5: *In the eigenfunction basis of Definition 3.3, the matrix A^R is block diagonal, with three by three blocks .*

Proof: First we investigate the matrix A^R_{EE}.

$$\begin{aligned} \big(A^R_{EE}\big)_{jk,mn} &= a_I\big((e_{jk},\mathbf{0},0,0),(e_{mn},\mathbf{0},0,0)\big) \;=\; i\omega\epsilon\big(e_{jk},e_{mn}\big)_R \\ &= i\omega\epsilon\int_{I_x^R}\Theta'_j\Theta'_m\,dx\int_{I_y^R}\Phi'_k\Phi'_n\,dy \\ &= i\omega\epsilon\;\;\lambda^x_j\lambda^y_k\;\;\mathcal{B}_{h_x^R}\big(\Theta_j,\Theta_m\big)\;\;\mathcal{B}_{h_y^R}\big(\Phi_k,\Phi_n\big) \\ &= i\omega\epsilon\;\;\lambda^x_j\lambda^y_k\;\;\delta_{jm}\delta_{kn}. \end{aligned}$$

The matrix A^R_{EE} is diagonal. For the block $A^R_{EH_x}$ we obtain

$$\begin{aligned} \big(A^R_{EH_x}\big)_{jk,mn} &= a_I\big((e_{jk},\mathbf{0},0,0),(0,\mathbf{h^x_{mn}},0,0)\big) = -\big(e_{jk},\operatorname{div}\mathbf{h^x_{mn}}\big)_R \\ &= -\int_{I_x^R}\Theta'_j\Theta'_m\;dx\int_{I_y^R}\Phi'_k\Phi'_n\;dy \\ &= -\lambda^x_j\lambda^y_k\;\;\delta_{jm}\delta_{kn}. \end{aligned}$$

For $A^R_{EH_y}$ the calculation is in principle the same, we only have to exchange Θ and Φ. Thus $A^R_{EH_x}, A^R_{EH_y}$ and due to symmetry of $a_I(u, v)$, $A^R_{H_xE}$ and $A^R_{H_yE}$ are diagonal. The coupling block between the $\mathbf{h}^x_{jk}$ reads as

$$\begin{aligned} \big(A^R_{H_xH_x}\big)_{jk,mn} &= a_I\big((0,\mathbf{h^x_{jk}},0,0),(0,\mathbf{h^x_{mn}},0,0)\big) \\ &= -i\omega\mu\big(\mathbf{h^x_{jk}}\mathbf{h^x_{mn}}\big)_R + \beta\big\langle\mathbf{h^x_{jk}}\cdot\mathbf{n_R},\mathbf{h^x_{mn}}\cdot\mathbf{n_R}\big\rangle_{\partial R} = -\lambda^y_k\;\;\delta_{jm}\delta_{kn} \end{aligned}$$

Hence, the matrix $A^R_{H_xH_x}$ is also diagonal. By exchanging Θ and Φ one can show that $A^R_{H_yH_y}$

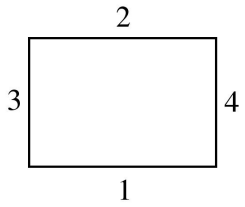

Figure 1. local edge numbering

has to be diagonal. Finally we have to investigate $A^R_{H_xH_y}$:

$$\begin{aligned}\left(A^R_{H_xH_y}\right)_{jk,mn} &= a_I\big((0,\mathbf{h^x_{jk}},0,0),(0,\mathbf{h^y_{mn}},0,0)\big)\\ &= -i\omega\mu\big(\mathbf{h^x_{jk}},\mathbf{h^y_{mn}}\big)_R + \beta\big\langle\mathbf{h^x_{jk}}\cdot\mathbf{n_R},\mathbf{h^y_{mn}}\cdot\mathbf{n_R}\big\rangle_{\partial R} \;=\; 0\end{aligned}$$

Due to symmetry of $a_I(u,v)$, $A^R_{H_yH_x}$ is also zero. Because the nine coupling blocks are zero or diagonal, the element matrix A^R can be written as a three by three block diagonal matrix, by reordering the degrees of freedom. □

For $i \le p_x+2$ and $j \le p_y+2$ the coupling elements between the coefficients of the three basis functions $e_{ij}, \mathbf{h^x_{ij}}$ and $\mathbf{h^y_{ij}}$ are collected in one of these three by three diagonal blocks. Elimination of the inner degrees of freedom is then equivalent to the inversion of three by three matrices. As basisfunctions with $i = p_x+2$ and $j = p_y+2$ are included only for notational convinience, the three by three block related to these degrees of freedom needs not to be inverted and these degrees of freedom can be set to zero. If either $i = p_x+2$ or $j = p_y+2$ only the diagonalelement belonging to $\mathbf{h^x_{ij}}$ and $\mathbf{h^y_{ij}}$, respectively, is different from zero and needs to be inverted. The coefficients of the other two basis functions are again zero according to the last remark.

3.2. *The bilinear form $a_{IF}(u,v)$*

In this section we take a closer look to the element matrix B^R of the rectangle R, which collects all the coupling elements of $a_{IF}(u,v)$ between the element facet and interior degrees of freedom. In the following, we use the local edge numbering according to Figure 1.

Our notation for the matrix blocks of B^R is similar to the previous subsection. For example for any boundary edge of the rectangle R with local number m, $\left(B^{R,m}_{H_xG_O}\right)_{jk,l}$ is the matrix element $\left(B^{R,m}_{H_xG_O}\right)_{(j(p_y+2)+k,l)}$ and $\left(B^{R,m}_{H_xG_O}\right)_{jk,l} = a_{IF}\big((0,\mathbf{0},0,g_{Ol}),(0,\mathbf{h^x_{jk}},0,0)\big)$, where g_{Ol} is supported on the local edge m.

On the horizontal edges 1 and 2 the vector functions $\mathbf{h^x_{ij}}$ are orthogonal to the outer normal vector. Hence, on these edges there is coupling only between the facet and the $\mathbf{h^y_{ij}}$ basis functions. We get for the local horizontal edge m

$$\left(B^{R,m}_{H_y\bullet}\right)_{jk,l} = s_k\left(1 \pm \beta\sqrt{\frac{\tilde{\epsilon}}{\mu}}\right)\int_{I^m}\Theta'_j\Xi'_l\,d\mathbf{x} \tag{11}$$

with the + sign for $\bullet = G_I$ and the − sign if $\bullet = G_O$. Furthermore $s_k = -\Phi_k(q^R_y)$ for local edge $m = 1$ and $s_k = \Phi_k(q^R_y + h^R_y)$ for $m = 2$. As s_k is a linear combination of the $Q^0_{I^m}$ and $Q^1_{I^m}$ expansion coefficients of Φ_k, the calculation of s_k does not require an evaluation of the integrated Legendre polynomials. On a uniform mesh, Θ_j and Ξ_l are basis functions of the same eigenvalue problem, and they are orthogonal. Thus

$$\int_{I^m} \Theta'_j \Xi'_l \, d\mathbf{x} = \delta_{jl} \, \lambda_j^x$$

which makes $B^{R,m}_{H_y\bullet}$ sparse.

On the vertical edges $m = 3, 4$ we have only nonzero matrix elements between the $\mathbf{h}^{\mathbf{x}}_{\mathbf{jk}}$ and the facet basis functions. We end up with

$$\left(B^{R,m}_{H_x\bullet}\right)_{jk,l} = s_j \left(1 \pm \beta \sqrt{\frac{\tilde{\epsilon}}{\mu}}\right) \int_{I^m} \Phi'_k \Xi'_l \, d\mathbf{y}. \tag{12}$$

Again $+$ is taken for $\bullet = G_I$ and $-$ for $\bullet = G_O$, and $s_j = -\Theta_j(q_x^R)$ for $m = 3$ and $s_j = \Theta_j(q_x^R + h_x^R)$ for $m = 4$. As for horizontal edges, s_j can be expressed by the $Q^0_{I^m}$ and $Q^1_{I^m}$ expansion coefficients of Θ_j. Using orthogonality of Φ_k and Ξ_l the integral simplifies to

$$\int_{I^m} \Phi'_k \Xi'_l \, d\mathbf{x} = \delta_{kl} \, \lambda_k^y.$$

3.3. *The bilinear form $a_F(u, v)$*

In this subsection we are going to find the matrix representation C of the bilinear form a_F, which describes the coupling between the facet degrees of freedom. Because each facet basis function is supported on one facet, there is no coupling between unknowns belonging to different facets. Writing C as blockmatrix, only the diagonal blocks C^{ii}, describing the coupling of the degrees of freedom of the facet F_i with themselves are nonzero.

As the notation for in and out going waves is related to a certain element it is not suitable for working with facet degrees of freedom. Instead it is more appropriate to denote the facet degrees of freedom as left and right going waves on vertical and as up and down going waves on horizontal facets. We will use the notation G_+ for up and right going waves, and G_- for left and down going waves, respectively. If the facet has local edge numbering 1 or 3 on an element (compare Figure 1) $G_+ = G_I$ and $G_- = G_O$, if it has local edge numbering 2 or 4, the situation is vice versa.

In the basis of Definition 3.4 the matrix C^{ii} has a block diagonal structure

$$C^{ii} = \begin{pmatrix} C^{ii}_{G_+G_+} & C^{ii}_{G_+G_-} \\ C^{ii}_{G_-G_+} & C^{ii}_{G_-G_-} \end{pmatrix} = \begin{pmatrix} \alpha_1 D(\tilde{\lambda}_k) & \alpha_2 D(\tilde{\lambda}_k) \\ \alpha_2 D(\tilde{\lambda}_k) & \alpha_3 D(\tilde{\lambda}_k) \end{pmatrix}. \tag{13}$$

Here $D(\tilde{\lambda}_k) \in \mathbb{C}^{(\tilde{p}+1)\times(\tilde{p}+1)}$ is a diagonal matrix with $D_{kk} = \tilde{\lambda}_k$. Depending on facet F_i , the parameter α is defined as

$$\alpha_1 = \alpha_3 = -\alpha_2 = 2\beta\frac{\tilde{\epsilon}}{\mu} \qquad \text{for } F_i \cap \partial\Omega = \emptyset$$

$$\alpha_1 = \alpha_3 = -\alpha_2 = \beta\frac{\tilde{\epsilon}}{\mu} \qquad \text{for } F_i \subset \Gamma_n$$

$$\alpha_1 = \alpha_3 = \left(\beta\frac{\tilde{\epsilon}}{\mu} - \sqrt{\frac{\tilde{\epsilon}}{\mu}}\right);\ \alpha_2 = \left(-\beta\frac{\tilde{\epsilon}}{\mu} - \sqrt{\frac{\tilde{\epsilon}}{\mu}}\right) \qquad \text{for } F_i \subset \Gamma_a$$

$$\alpha_1 = \left(\beta\frac{\tilde{\epsilon}}{\mu} \pm 2\sqrt{\frac{\tilde{\epsilon}}{\mu}}\right);\ \alpha_2 = -\beta\frac{\tilde{\epsilon}}{\mu};\ \alpha_3 = \left(\beta\frac{\tilde{\epsilon}}{\mu} \mp 2\sqrt{\frac{\tilde{\epsilon}}{\mu}}\right) \qquad \text{for } F_i \subset \Gamma_d.$$

The sign in α_1 and α_3 in the last line depends on wether the incident wave onto the domain is represented by G_+ or by G_-.

4. Solving the system of equations

Summarizing the last section, we end up with the following linear system of equations

$$\begin{pmatrix} A & B \\ B^T & C \end{pmatrix} \begin{pmatrix} \mathbf{u}_{inner} \\ \mathbf{u}_{facet} \end{pmatrix} = \begin{pmatrix} \mathbf{0} \\ \mathbf{f} \end{pmatrix}$$

where the element matrices A^R and B^R are collected in A and B, respectively. $\mathbf{u}_{inner}$ represents the inner degrees of freedom, and the facet degrees of freedom are collected in $\mathbf{u}_{facet}$. When solving the linear system of equations we first eliminate all the interior degrees of freedom and solve the resulting system for the facet degrees of freedom

$$S\,\mathbf{u}_{facet} = \mathbf{f} \qquad \text{with} \qquad S = C - B^T A^{-1} B. \tag{14}$$

First, let us take a closer look onto the structure of the Schur complement matrix S, especially onto $B^T A^{-1} B$. Because inner basisfunctions are supported only on a single element, A does not couple inner degrees of freedom belonging to different elements. B describes the coupling between the element degrees of freedom and the degrees of freedom belonging to its edges. Consequently, the Schur complement matrix S has coupling blocks only between facets, which are edges of the same element. Hence, interior facets couple apart from themselves to two parallel edges and to four perpendicular edges, whereas boundary facets couple to one parallel facet and to two perpendicular ones. Using the structures of A and B, it is obvious that the coupling blocks between parallel edges and with the edge itself (the diagonal block) have a two by two blockdiagonal structure. The coupling blocks to perpendicular edges are full.

We solve the Schur complement system (14) with a preconditioned conjugate gradient method (PCG), using the complex symmetric inner product $\mathbf{x}^T\mathbf{y}$. Although this method works well in our numerical examples, there exists no rigorous convergence analysis. As a preconditioner, an additive Schwartz-type method is used. The preconditioner P has the structure

$$P = \sum \left(P^{ii}\right)^{-1}$$

where P^{ii} describes the coupling of degrees of freedom on facet i with themselves, and it is equal to the corresponding diagonal block in the Schur complement matrix S. Writing P^{ii} as two by

two block matrix

$$P^{ii} = \begin{pmatrix} P^{ii}_{G_+G_+} & P^{ii}_{G_+G_-} \\ P^{ii}_{G_-G_+} & P^{ii}_{G_-G_-} \end{pmatrix}, \tag{15}$$

these blocks can be computed for inner horizontal facets with

$$\begin{aligned}
P^{ii}_{G_+G_+} &= C^{ii}_{G_+G_+} - \left(B^{R,1}_{H_yG_I}\right)^T \left(A^R_{H_yH_y}\right)^{-1} B^{R,1}_{H_yG_I} - \left(B^{R,2}_{H_yG_O}\right)^T \left(A^R_{H_yH_y}\right)^{-1} B^{R,2}_{H_yG_O} \\
P^{ii}_{G_+G_-} &= C^{ii}_{G_+G_-} - \left(B^{R,1}_{H_yG_I}\right)^T \left(A^R_{H_yH_y}\right)^{-1} B^{R,1}_{H_yG_O} - \left(B^{R,2}_{H_yG_O}\right)^T \left(A^R_{H_yH_y}\right)^{-1} B^{R,2}_{H_yG_I} \\
P^{ii}_{G_-G_+} &= C^{ii}_{G_-G_+} - \left(B^{R,1}_{H_yG_O}\right)^T \left(A^R_{H_yH_y}\right)^{-1} B^{R,1}_{H_yG_I} - \left(B^{R,2}_{H_yG_I}\right)^T \left(A^R_{H_yH_y}\right)^{-1} B^{R,2}_{H_yG_O} \\
P^{ii}_{G_-G_-} &= C^{ii}_{G_-G_-} - \left(B^{R,1}_{H_yG_O}\right)^T \left(A^R_{H_yH_y}\right)^{-1} B^{R,1}_{H_yG_O} - \left(B^{R,2}_{H_yG_I}\right)^T \left(A^R_{H_yH_y}\right)^{-1} B^{R,2}_{H_yG_I}.
\end{aligned} \tag{16}$$

For inner vertical facets we get

$$\begin{aligned}
P^{ii}_{G_+G_+} &= C^{ii}_{G_+G_+} - \left(B^{R,3}_{H_xG_I}\right)^T \left(A^R_{H_xH_x}\right)^{-1} B^{R,3}_{H_xG_I} - \left(B^{R,4}_{H_xG_O}\right)^T \left(A^R_{H_xH_x}\right)^{-1} B^{R,4}_{H_xG_O} \\
P^{ii}_{G_+G_-} &= C^{ii}_{G_+G_-} - \left(B^{R,3}_{H_xG_I}\right)^T \left(A^R_{H_xH_x}\right)^{-1} B^{R,3}_{H_xG_O} - \left(B^{R,4}_{H_xG_O}\right)^T \left(A^R_{H_xH_x}\right)^{-1} B^{R,4}_{H_xG_I} \\
P^{ii}_{G_-G_+} &= C^{ii}_{G_-G_+} - \left(B^{R,3}_{H_xG_O}\right)^T \left(A^R_{H_xH_x}\right)^{-1} B^{R,3}_{H_xG_I} - \left(B^{R,4}_{H_xG_I}\right)^T \left(A^R_{H_xH_x}\right)^{-1} B^{R,4}_{H_xG_O} \\
P^{ii}_{G_-G_-} &= C^{ii}_{G_-G_-} - \left(B^{R,3}_{H_xG_O}\right)^T \left(A^R_{H_xH_x}\right)^{-1} B^{R,3}_{H_xG_O} - \left(B^{R,4}_{H_xG_I}\right)^T \left(A^R_{H_xH_x}\right)^{-1} B^{R,4}_{H_xG_I}
\end{aligned} \tag{17}$$

with the blocks of A^R defined in (10), the blocks of B^R defined in (11) and (12) and the C^{ii} from (13). For boundary edges we only have to consider one of the two summands, which one depends if the neighboring element is on the righthand (upper) or lefthand (lower) side of the edge.
By the structure of the A^R, B^R, and C^{ii} the four blocks of P^{ii} are diagonal, and therefore very cheap to invert.

5. Hanging Nodes

There are several disadvantages of the approach discussed above. For example, a very fine mesh is required for a good approximation of an arbitrary domain. This is undesirable, as regions where ϵ is constant are meshed with fine elements, even though large elements with high order basis functions are more appropriate. Furthermore refinement to specific points of the mesh, where singularities of the solution are expected, is not possible at all.

5.1. *The Mesh*

One way to handle this problem is to use a rectangular mesh with hanging nodes. For a rectangular mesh with hanging nodes, the interior degrees of freedom can be eliminated in a similar manner as for a uniform rectangular mesh. The major difference is, that the eigenvalue problem has to be solved for each element size and polynomial order appearing in the mesh. Consequently it is convenient to use only a small number of different sized elements. Therefore, an element, which needs to be refined, is devided into four equally sized elements with the polynomial orders p_x and p_y chosen as half of the polynomial orders of the original element. With this strategy the total number of unknowns during the refinement process is kept approximately constant. Let h_x and h_y be the dimensions of the element in the initial uniform mesh. Then element dimensions after n refinement steps are $\left(\frac{1}{2}\right)^n h_x$ and $\left(\frac{1}{2}\right)^n h_y$. Hence if the polynomial order of the initial uniform mesh was constant, in the worst case n eigensolutions are required.

Figure 2 illustrates a simple mesh after a few refinement steps. During the refinement of one element each of the long boundary facets in $\mathcal{F}$ is exchanged by the two new ones. Thus the shaded

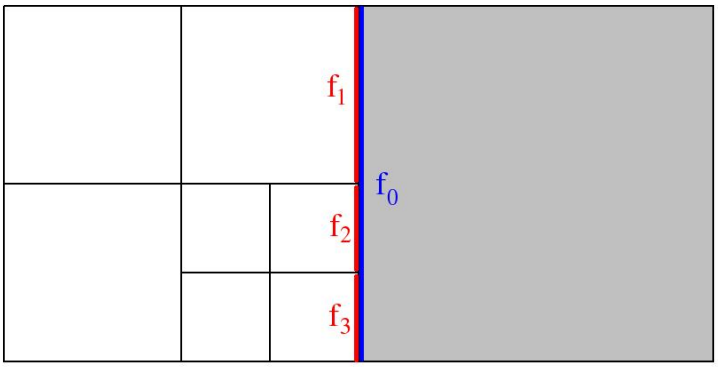

Figure 2. a mesh with hanging nodes

element in the mesh of Figure 2 has instead of the blue facet f_0 the three boundary edges f_1, f_2 and f_3, plotted in red. As for the uniform mesh, the facet basisfunctions are derivatives of the eigenfunctions of Problem 3.

5.2. *The coupling between facet and interior degrees of freedom*

In the hanging node case the matrix representations of the bilinear forms $a_I(u,v)$ and $a_F(u,v)$ are similar to the uniform case, but for the bilinear form $a_{IF}(u,v)$ the situation is different. Here the coupling blocks between the inner degrees of freedom and the facet degrees of freedom of a hanging node edge are not sparse anymore. In the following we will demonstrate this for a horizontal hanging node edge with local number f of the element R according to (8). The interior basis functions of R are according to Definition 3.3, and the facet with its basis functions obeys Definition 3.4. We assume that the hanging node facet f is a facet of level n, thus its length is $\tilde{h} = (1/2)^n h_x^R$.

Inserting the basis functions into the bilinear form a_{IF}, we end up with the coupling block $B^{R,f}_{H_y\bullet}$ from (11). The difference to the uniform mesh case is, that now Θ_j and Ξ_l are solutions of different eigenvalue problems, and consequently they are not orthogonal anymore. In the following we will examine the integral $\int_{I^f} \Theta_j' \Xi_l' \, d\mathbf{x}$ more closely. Therfore we assume that facet f with $I^f = I_n$ and order $\tilde{p} = p_n$ arises after n refinement steps from $I_0 = I_x^R$ with polynomial order $p_0 = p_x^R$. After refinement step k we obtain a facet with $I_k = [q_k, q_k + h_k]$ and order p_k from the facet with I_{k-1}, where $h_k = \frac{1}{2} h_{k-1}$, q_k either equals q_{k-1} or $q_{k-1} + h_k$ and the polynomial order $p_k = \frac{1}{2} p_{k-1}$.

With the corresponding eigenvector $\mathbf{\Theta}_j$ of Θ_j and $\mathbf{\Xi}_l$ of Ξ_l obtained from Problem 3.2, and the matrices $E \in \mathbb{C}^{(p_0+1)\times(p_0+1)}, \tilde{E} \in \mathbb{C}^{(p_n+1)\times(p_n+1)}$ with $E_{jk} = (\mathbf{\Theta}_j)_k$ and $\tilde{E}_{lk} = (\mathbf{\Xi}_l)_k$, respectively, we can express as in (9) Θ_j' and Ξ_l' by the Legendre polynomials

$$\int_{I^f} \Theta_j' \Xi_l' \, d\mathbf{x} = \frac{4}{h_0 h_n} \sum_{m=1}^{p_0+1} \sum_{q=1}^{p_n+1} E_{jm} \tilde{E}_{lq} \int_{I^f} L_{I_0}^{m-1} L_{I_n}^{q-1} \, d\mathbf{x}.$$

Next we introduce the transformation matrices $T_k^+, T_k^- \in \mathbb{C}^{(p_{k-1}+1)\times(p_k+1)}$ with

$$\left(T_k^+\right)_{ij} = (2j-1) \int_0^1 L_{[-1,1]}^{i-1} L_{[0,1]}^{j-1} \, dx$$

$$\left(T_k^-\right)_{ij} = (2j-1) \int_{-1}^0 L_{[-1,1]}^{i-1} L_{[-1,0]}^{j-1} \, dx.$$

With these matrices we can approximate Legendre polynomials $L^{i-1}_{I_{k-1}}$ by Legendre polynomials on I_k:

$$L^{i-1}_{I_{k-1}} = \sum_{j=1}^{p_k+1} \frac{2j-1}{h_k} \left(\int_{I_k} L^{i-1}_{I_{k-1}} L^{j-1}_{I_k} \, dx \right) L^{j-1}_{I_k} = \sum_{j=1}^{p_k+1} \left(T^{\pm}_k\right)_{ij} L^{j-1}_{I_k}$$

Here we take T^-_k if $q_k = q_{k-1}$ and T^+_k else. Doing this step by step, $L^{m-1}_{I_0}$ can be approximated by the polynomials $L^{q-1}_{I_n}$, and we end up with

$$\int_{I^f} \Theta'_j \Xi'_l \, d\mathbf{x} = \frac{4}{h_0 h_n} \sum_{s=1}^{p_n+1} \sum_{q=1}^{p_n+1} \left(E \prod_{k=1}^{n} T^{\pm}_k \right)_{js} \tilde{E}_{lq} \int_{I_f} L^{s-1}_{I_n} L^{q-1}_{I_n} \, d\mathbf{x}.$$

If we use now orthogonality relations between the Legendre polynomials, the integral simplifies to

$$\int_{I^f} \Theta'_j \Xi'_l \, d\mathbf{x} = \frac{2}{h_0} \left(E \left(\prod_{k=1}^{n} T^{\pm}_k \right) D \tilde{E}^T \right)_{jl}.$$

Here $D \in \mathbb{C}^{(p_n+1)\times(p_n+1)}$ is a diagonal matrix with $D_{ii} = \frac{2}{2i-1}$.

The coupling blocks of vertical edges can be treated in a similar fashion. Note that these blocks are full, and consequently all the coupling blocks of the Schur complement matrix between edges of the same element are full, too.

5.3. *The Preconditioner*

In order to solve the resulting linear system, we again use an additive Schwartz preconditioner with a PCG iteration. The additive preconditioner is block diagonal and it is constructed from blocks P^{ii} in a similar manner to the uniform case.

In the case of a edge with a hanging node as either of its endpoints, the edge to edge coupling block of the Schur complement matrix is full. In this case the block P^{ii} is constructed by treating the facet F as if neither of its endpoints is a hanging node and the rectangles R_1, R_2 surrounding the facet share polynomial order with the facet. Following this strategy the set of eigenfunctions Φ_k (if F is vertical) and Θ_j (if F is horizontal), respectively, needed for the basisfunctions of R_1 and R_2, is equal to the set of Ξ_l, which is used for the construction of the facet basis functions. Hence we get for the integrals $\int_{I^F} \Phi_k \Xi_l \, d\mathbf{x} = \delta_{kl}\lambda_k$ in (12) and $\int_{I^F} \Theta_j \Xi_l \, d\mathbf{x} = \delta_{jl}\lambda_j$ in (11), respectively. Consequently the "modified" blocks B^R in the construction of the preconditioner (16) and (17) are no longer full, like for building up the Schur complement matrix. With this approach, the four blocks of P^{ii} are again diagonal. Inversion of P is then equivalent to the inversion of a block diagonal matrix, with two by two blocks. Note that for edges, with neither of the endpoints a hanging node, P^{ii} is equal to the corresponding block in the Schur complement matrix. Applying the preconditioner is then equivalent to the inversion of the degrees of freedom on this edge.

6. Results

The following numerical results were computed on a square domain $\Omega = (0,2)^2$. Absorbing boundary conditions with $E_{in} = \exp\left(-\frac{(y-1)^2}{0.1}\right)$ on edge $x = 0$ and $E_{in} = 0$ elsewhere were

β	$\frac{1}{5}$	$\frac{1}{4}$	$\frac{1}{3}$	$\frac{1}{2}$	1	2	3	4	5
$\epsilon = \frac{1}{16}$	95	89	81	76	66	54	44	40	44
$\epsilon = \frac{1}{4}$	120	105	94	78	59	41	51	55	58
$\epsilon = 1$	140	121	102	73	35	54	79	88	103
$\epsilon = 4$	108	86	62	34	65	99	151	194	239
$\epsilon = 16$	50	34	47	70	131	317	597	919	1366

Table 1. iteration numbers for different values of ϵ and β

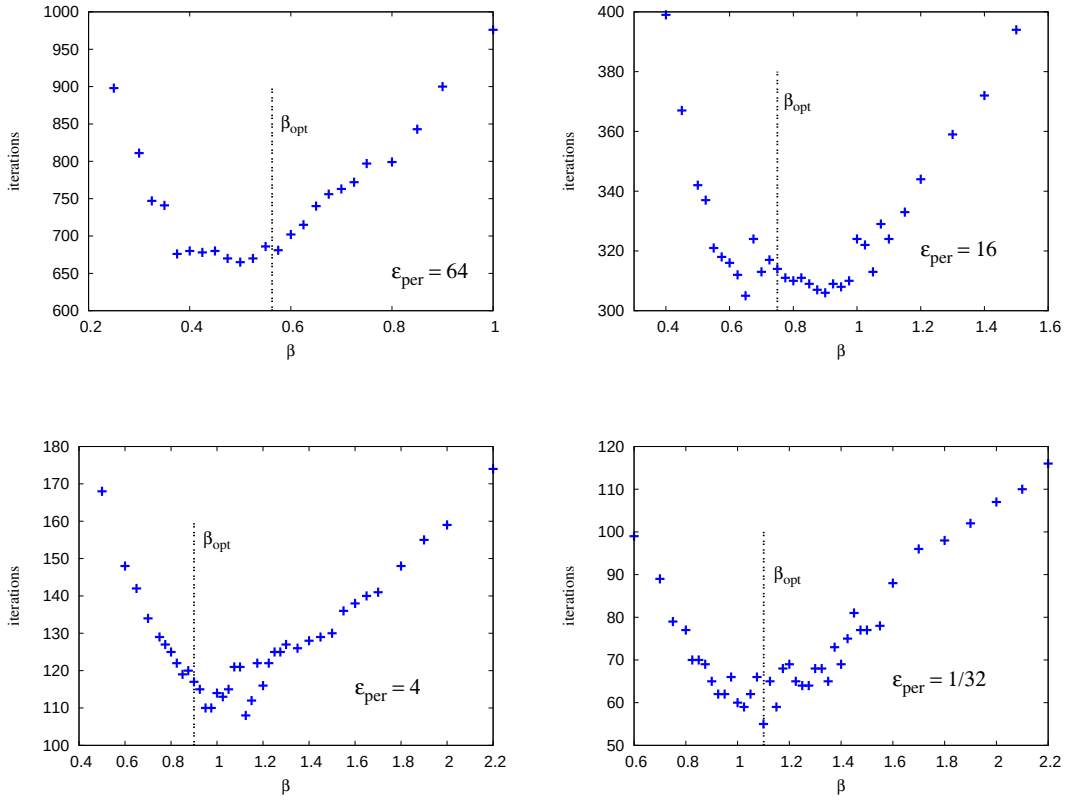

Figure 3. The figure shows the number of iterations for different stabilization parameters β. In the four plots we vary the value of ϵ in the perturbed region, and choose $\epsilon_{per} = 64$ (top left), $\epsilon_{per} = 16$ (top right), $\epsilon_{per} = 4$ (bottom left) and $\epsilon_{per} = \frac{1}{32}$ (bottom right)

posed on the boundary edges. The physical interpretation of this problem is a wave incoming from the lefthand side with a Gaussian amplitude.

We begin this section by studying the dependency between the number of iterations required to solve the linear system (14) with the preconditioned iterative scheme presented in section 4 and the value of the stabilization parameter β. First, we will consider a constant ϵ on a uniform mesh of 4×4 elements with polynomial order 50 in both spatial directions and $\mu = 1$, $\omega = 10\pi$. The number of iterations required to solve this problem for different values of ϵ and β are given in Table 1.

Based on these results, the best choice for the stabilization parameter is $\beta = \sqrt{\mu/\epsilon}$, which corresponds to our previous observations in Section 2. Choosing this β eliminates the coupling terms between the outgoing waves and the inner degrees of freedom on a each element. In this case, the fields in the interior of the element depend only on the incoming waves, and couple via the incoming waves to the outgoing waves. Furthermore we observe, that the number of iterations for large values of ϵ is very sensitive to the choice of the parameter β.

Finding a good value for β is even more crucial if ϵ is not constant. One way to choose β

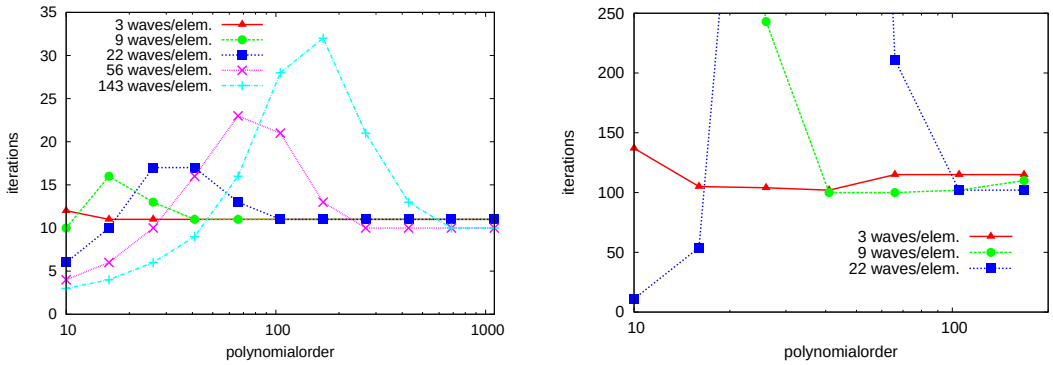

Figure 4. In both plots, the red, green, blue, magenta and cyan lines represent values of ω such that the size of one element is 3, 9, 22, 56 and 143 wavelength, respectively. With an underlaying mesh of 2 times 2 element for the lefthand plot, this results in values of $\omega = 6\pi$, 18π, 44π, 106π and 286π. For the righthand plot the mesh consists of 12 times 12 elements, and therfore $\omega = 36\pi$, 108π and 264π.

would be to take use elementwise constant $\beta_{|_R} = \sqrt{\mu/\tilde{\epsilon}}$. However, this choice fits poorly to the presented method. As the eigenvalue Problem 3 depends on the stabilizing parameter, it has to be solved for each element with different value of β, regardless of the size. Furthermore, if β has different value on two neighboring elements, the coupling blocks between at least the inner degrees of freedom of one element and the edge degrees of freedom of the common edge are full. Therfore, β is best chosen as a global constant.

In order to demonstrate the dependence of the number of iterations on the value of β we choose $\mu = 1, \omega = 15\pi$ and consider a piecewise constant ϵ

$$\epsilon = \begin{cases} \epsilon_{per} & \text{for } \mathbf{x} \in (1, \frac{5}{3}) \times (\frac{1}{3}, 1) \\ 1 & \text{else} \end{cases},$$

where the value of the perturbation ϵ_{per} is varied. A uniform mesh of 6×6 elements and polynomial order 120 in both directions is considered. Such a mesh conforms to the perturbation, which is of the size of four elements. In Figure 3 the number of required iterations is plotted for different values of ϵ_{per} and β.

Motivated by the previous results, we propose to choose the global constant β as

$$\beta_{opt} = \sqrt{\frac{\mu}{\hat{\epsilon}}},$$

where $\hat{\epsilon}$ can be interpreted as effective ϵ of the domain. Based on our experiences, a good value for $\sqrt{\hat{\epsilon}}$ is the mean value of $\sqrt{\epsilon}$

$$\sqrt{\hat{\epsilon}} = \frac{1}{A} \int_\Omega \sqrt{\epsilon}\, d\mathbf{x}$$

on the computational domain Ω with area A. Figure 3 shows, that using this definition is a good choice for the stabilizing constant. Apart from this, we should mention that the number of iterations increases with increasing ϵ.

Next we investigate the dependence of the number of iterations on the frequency ω and the polynomial order for different uniform meshes. In the following simulations ϵ, μ and β were chosen to be one. In Figure 4, the number of iterations is plotted against the polynomial order in one spatial direction for different values of the wavelength. From these plots we conclude that for a

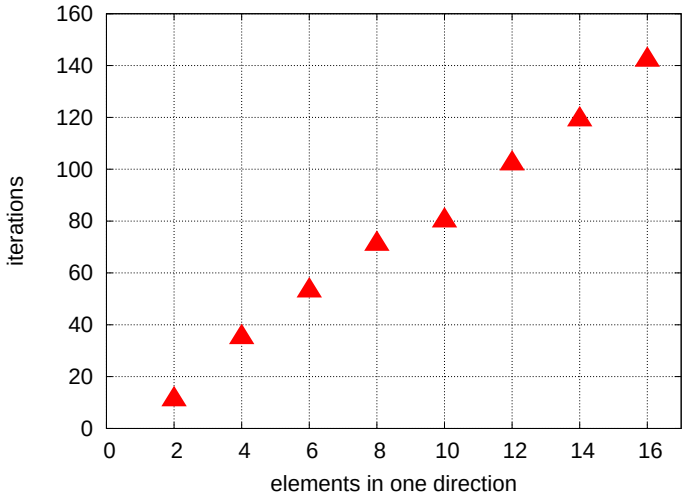

Figure 5. number of iterations for different uniform meshes

polynomial order far too small to resolve the solution, a small number of iterations is required to get a solution. When the polynomial order is increased, the number of iterations grows very rapidly, or the solver does not converge at all. At a polynomial order between three and four times the number of waves per element the number of iterations drops down to a minimum, and we are able to resolve the solution. This goes along with literature. From (*1*) we know, that at least π unknowns per wavelength are needed to resolve the wave. A further increase of the polynomial order leads only to a small growth in the number of iterations. Moreover, the number of iterations at the minimum depends on the mesh, but it seems to be almost independent of ω. For 2 times 2 elements we need about 10 iterations, for 12 times 12 elements about 100 iterations are necessary.

In Figure 5 we study the dependence of the number of iterations on the element size in a uniform mesh. The angular frequency was chosen such that the size of each element is 22 wavelengths. The polynomial order was chosen as 105 for both spatial directions, which is equivalent to about 4 unknowns per wavelength. From Figure 5, one can observe that when the solution can be resolved, the number of iterations is proportional to the number of elements in one spatial direction. Our interpretation of this observation is that the incoming wave, fixed by the function E_{in} on the lefthand boundary of the computational domain, requires a constant number of iterations to "propagate" through one element. Based on Figure 4 the number of iterations seems to be almost independent of the angular frequency for meshes with three or more degrees of freedom per wavelength, hence we conclude that this "speed of propagation" is independent of this quantity.

Figure 6 illustrates the computational times for a uniform mesh of 4 times 4 elements, and a mesh of 8 times 8 elements for different polynomial orders. All the computations were done on an Intel 2 GHz processor. The angular frequency was chosen such that the size of each element was nine wavelengths. Figure 5 shows that for a polynomial order p the solution process and the set up of the matrices has the complexity $\mathcal{O}(p^2)$. Since the number of iterations increases very slowly if the wave can be resolved, the time per iteration is of order p^2. For polynomial orders less than 30 the discretization could not resolve the solution and a large number of iterations was required. In Figure 6 this is seen as a perturbation of the computational times. Although the dependence of the eigenvalue problem is of an higher order than p^2, for relevant polynomial orders the solution of the eigenvalue problem is much faster than the solution process.

Next, we will consider a mesh with hanging nodes. The computational domain and the bound-

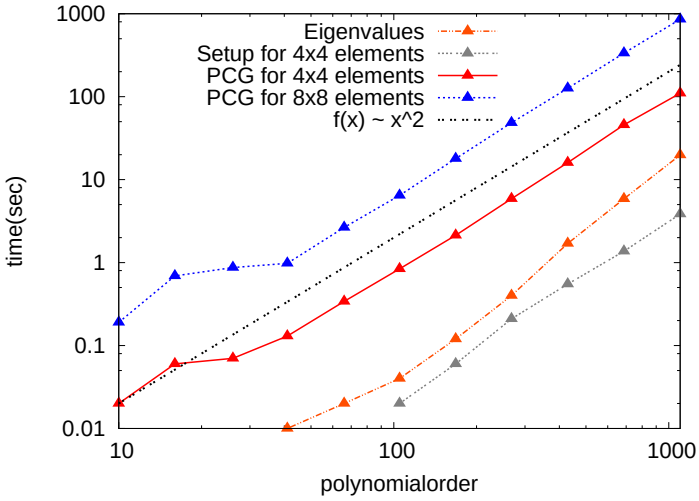

Figure 6. computational times for 4×4 and 8×8 elements

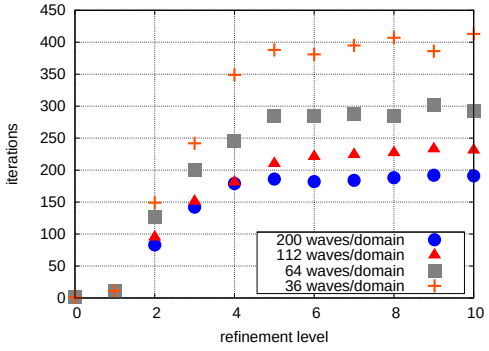

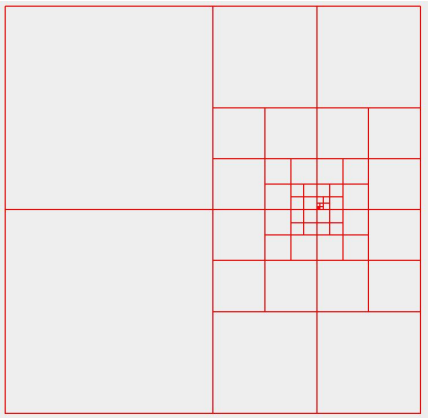

Figure 7. number iterations for different refinement levels and wavelength (left) and the hanging nodes mesh of refinement level 10 (right)

ary conditions are the same as for the previous test cases. The mesh was generated from a single element (refinement level zero) by refining towards the point $P = (1.51, 1.01)$. The following refinement strategy was used: in each refinement step, an element is divided into four equally sized elements, if it contains the point P. In view of approximation properties, we want to avoid arbitrary level hanging nodes. Therfore we also refine elements with edge length h, if the point P is within a distance $c\,h$ from the element. The constant c defines indirectly the maximal level of the hanging nodes, which is allowed on the edge. Figure 7 shows tenth level mesh, consisting of 61 elements, which was generated with $c = 0.1$.

On this mesh, we studied the dependence of the number of iterations on the refinement level and angular frequency ω. Independently of the angular frequency, we observe the same features. For small refinement levels, the number of iterations increases rapidely with increasing refinement level. At refinement level five, the number of iterations reaches a constant level. As discussed above, in the uniform mesh case (refinement level one) the number of iterations seems to be independent of the angular frequency. This is no longer true in the hanging node case. For a growing angular frequency, which is equivalent to an increase of the number of waves in the domain, the number of iterations grows as well.

We conclude the result section with a large scale problem. We assume that an incoming wave

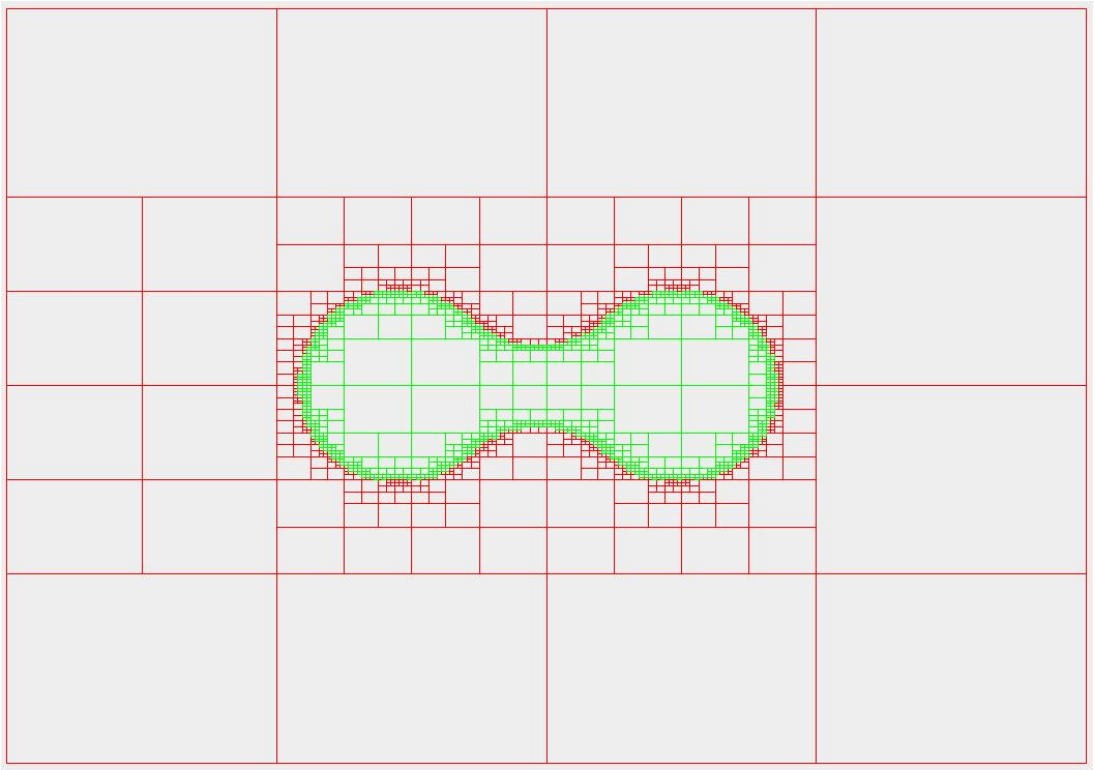

Figure 8. mesh of the domain with obstacle

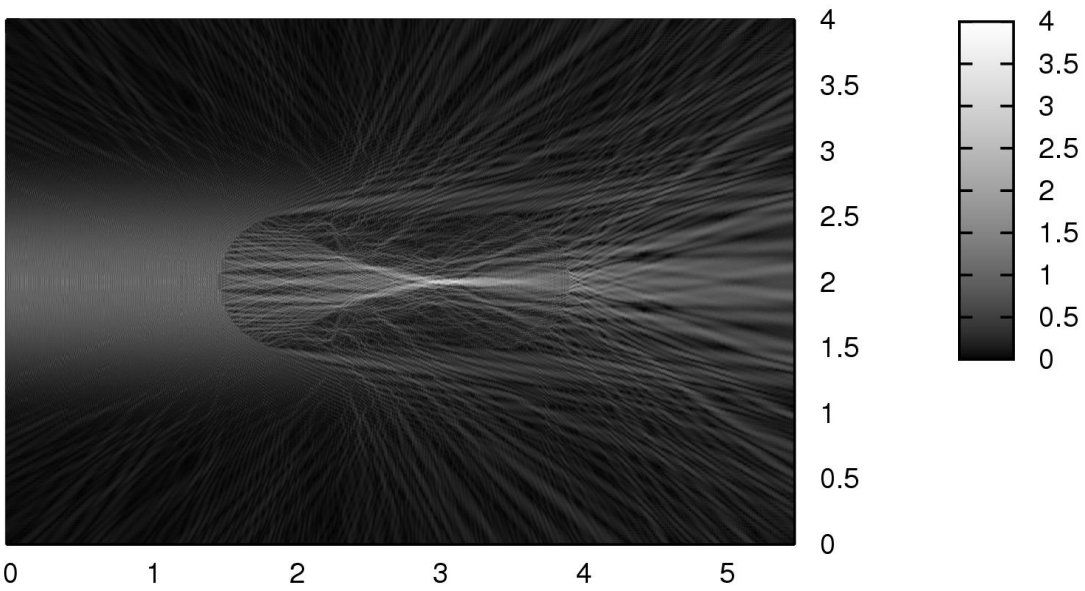

Figure 9. amplitude of the solution for scattering at an obstacle

with an Gauss error distribution shaped amplitude is scattered at an obstacle. The computational domain is a rectangle with the dimension $(0, 5.5) \times (0, 4)$. In order to enforce an incoming wave from left, we set $E_{in} = \exp\left(-\frac{(y-2)^2}{0.4}\right)$ for $x = 0$ and $E_{in} = 0$ elsewhere. The shape of the obstacle is visualized in green in the mesh of the computational domain in Figure 8. The obstacle has a length of 4.8, and its width is 2. We assume ϵ to be one in the background (red area of the mesh) and two in the obstacle. Choosing $\omega = 80\pi$ results in an effective length of 135 wavelength of the obstacle. We started the meshing process with one single element covering the rectangular

domain (refinement level zero). In each refinement step, the actual mesh is refined towards the boundary of the obstacle. More precisely, in each refinement step, an element with edge lenght h and polynomial order p is divided into four smaller elements with a polynomial order $\frac{p}{2}$, if the boundary of the obstacle crosses the element, or if the distance between element and the boundary is smaller than $c\,h$ with the constant $c = 0.1$. After 8 refinement steps, we obtained the mesh of Figure 8 contains 1588 elements. The polynomial order of the refinement level zero was 1250 into each spatial direction. The largest elements in the mesh are of level two, and they have consequently polynomial order 313. The level eight elements near the interface are of order five.

In Figure 9 the amplitude, or more precisely the absolute value of the field E is plotted. These results were obtained on an Intel 2 GHz processor. The solution of the eigenvalue problems was done in 0.73 seconds, and the set up procedure took 6.97 seconds. The most time consuming part was the solution process. For the 1835 iterations 2912 seconds were necessary.

References

(1) M. Ainsworth Discrete dispersion relation for *hp*-version finite element approximation at high wavenumber *SIAM J. Numer. Anal.*, 42 (2004), pp.553–575.
(2) M. Ainsworth and K. Pinchedez *hp*-approximation theory for BDFM and RT finite elements on quadrilaterals *SIAM J. Numer. Anal.*, 40 (2002), pp.2047–2068.
(3) D.N. Arnold, F. Brezzi, B. Cockburn and L.D. Marini Unified Analysis of discontinuous Galerkin methods for elliptic problems *SIAM J. Numer. Anal.*, 39 (2002), pp.1749–1779.
(4) I. Babuska and J.M. Melenk The partition of unity method *J. Numer. Meth. Engrg.*, 40 (1997), pp.727–758.
(5) I. Babuska and M. Suri The p and $h-p$ versions of the finite element method, basic principles and properties *SIAM Rev.*, 36 (1994), pp.578–632.
(6) F. Brezzi and M. Fortin *Mixed and hybrid finite element methods,* Springer, New York, 1991.
(7) O. Cessenat and B. Després Application of the ultra weak variational formulation of elliptic PDEs to the two dimensional Helmholtz problem *SIAM J. Numer. Anal.*, 35 (1998), pp.255–299.
(8) O. Cessenat and B. Després Using plane waves as base functions for solving time harmonic equations with the ultra weak variational formulation *J. Computational Acoustics*, 11 (2003), pp.227–238.
(9) S.N. Chandler-Wilde and A.T. Peplow, A boundary integral formulation for the Helmholtz equation in a locally perturbed half plane, *Z. Angew. Math. Mech.*, 85 (2005), pp.79–88.
(10) P. Ciarlet *The finite element method for elliptic problems* North-Holland, Amsterdam, 1978
(11) B. Cockburn and J. Gopalakrishnan A characterization of hybrid mixed methods for second order elliptic problems *SIAM J. Numer. Anal.*, 42 (2004), pp.283–301.
(12) B. Cockburn, J. Gopalakrishnan and R. Lazarov Unified hybridization of discontinuous Galerkin, mixed and continuous Galerkin methods for second order elliptic problems *SIAM J. Numer. Anal.*, 47 (2009), pp.1319–1365.
(13) D. Colton and R. Kress, *Integral Equation Methods in Scattering Theory,* Krieger Pub. Co., Malabar, FL, 1991.
(14) L. Demkowicz *Computing with hp-adaptive finite elements. I. one and two dimensional elliptic and maxwell problems* Chapman & Hall / CRC Press, Boca Raton, FL, 2006
(15) Y.A Erlangga, C Vuik and C.W Oosterlee On a class of preconditioners for solving the Helmholtz equation Appl. Numer. Math., 50 (2004), pp. 409–425
(16) C. Farhat, I. Harari and U.A. Hetmaniuk A discontinuous Gelerkin method with Lagrange multipliers for the solution of Helmholtz problems in the mid-frequency regime *Comput. Methods Appl. Mech. Engrg.*, 192 (2003), pp.1389–1419.
(17) I. Harari and E. Turkel, Accurate Finite Difference Methods for Time Harmonic Wave Propagation, *J. Comp. Phys.*, 119 (1995), pp.252–270.
(18) F. Ihlenburg and I. Babuska, Finite element solution of the Helmholtz equation with high wave number part II: The $h-p$ Version of the FEM, *SIAM J. Numer. Anal.*, 34 (1997), pp.315–358.
(19) F. Ihlenburg *Applied mathematical sciences Vol. 132: finite element analysis of acoustic scattering,* Springer, Berlin, 1998.
(20) C. Le Potier and R. Le Martret, Finite volume solution for Maxwell's equations in nonsteady mode, *La Recherche Aérospatiale*, 5 (1994), pp.329–342.
(21) Z.C. Li, The Trefftz method for Helmholtz equation with degeneracy, *Appl. Num. Math.*, 58 (2008), pp.131–159.
(22) P. Monk, J. Schöberl and A. Sinwel, *Hybridizing Raviart-Thomas Elements for the Helmholtz Equation*, RICAM-Report 2008-22, Johann Radon Institute for Computational and Applied Mathematics, Linz, 2008.
(23) P. Monk and D.Q. Wang A least-squares method for the Helmholtz equation *Comput. Methods Appl. Mech. Engrg.*, 175 (1999), pp.121–136.
(24) C. Schwab *p− and hp−finite element methods, theory and applications in solid and fluid mechanics* Oxford University Press, New York, 1998